Field-Effect Transistors Based on Few-Layered α-$MoTe_2$

Nihar R. Pradhan,[†] Daniel Rhodes,[†] Simin Feng,[‡] Yan Xin,[†] Shahriar Memaran,[†] Byoung-Hee Moon,[†] Humberto Terrones,[§] Mauricio Terrones,[‡] and Luis Balicas[†,*]

[†]National High Magnetic Field Lab, Florida State University, 1800 E. Paul Dirac Drive, Tallahassee, Florida 32310, United States, [‡]Department of Physics and Department of Materials Science and Engineering and Materials Research Institute, The Pennsylvania State University, University Park, Pennsylvania 16802, United States, and [§]Department of Physics, Applied Physics, and Astronomy Rensselaer Polytechnic Institute, 110 Eighth Street, Troy, New York 12180-3590, United States

ABSTRACT Here we report the properties of field-effect transistors based on a few layers of chemical vapor transport grown α-$MoTe_2$ crystals mechanically exfoliated onto SiO_2. We performed field-effect and Hall mobility measurements, as well as Raman scattering and transmission electron microscopy. In contrast to both MoS_2 and $MoSe_2$, our $MoTe_2$ field-effect transistors are observed to be hole-doped, displaying on/off ratios surpassing 10^6 and typical subthreshold swings of ~140 mV per decade. Both field-effect and Hall mobilities indicate maximum values approaching or surpassing 10 $cm^2/(V\ s)$, which are comparable to figures previously reported for single or bilayered MoS_2 and/or for $MoSe_2$ exfoliated onto SiO_2 at room temperature and without the use of dielectric engineering. Raman scattering reveals sharp modes in agreement with previous reports, whose frequencies are found to display little or no dependence on the number of layers. Given that MoS_2 is electron-doped, the stacking of $MoTe_2$ onto MoS_2 could produce ambipolar field-effect transistors and a gap modulation. Although the overall electronic performance of $MoTe_2$ is comparable to those of MoS_2 and $MoSe_2$, the heavier element Te leads to a stronger spin–orbit coupling and possibly to concomitantly longer decoherence times for exciton valley and spin indexes.

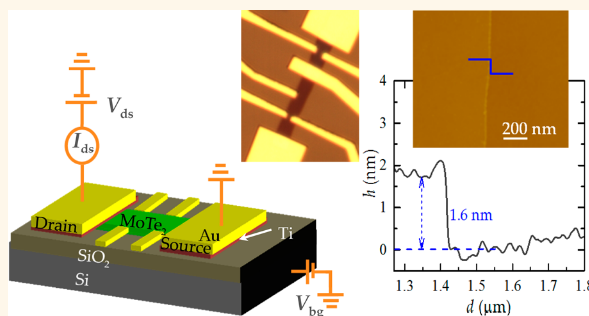

KEYWORDS: two-dimensional atomic layers · transition metal dichalcogenides · field-effect transistors · carrier mobility · Raman scattering

Several semiconducting transition metal dichalcogenides (TMX_2, where TM = Mo, W, Re, Nb, *etc*., and X = S, Se, Te) crystallize in the layered trigonal prismatic structure characterized by a weak van der Waals interplanar coupling, strong in-plane covalent bonding, lack of inversion symmetry, and a strong spin–orbit coupling.[1] In the single-layered form, MoS_2 was found to be a direct gap semiconductor with energy gaps located at the K and K′ points of the Brillouin zone. Both the highest valence bands and the lowest conduction bands are formed primarily from the Mo d-orbitals.[2] The large spin–orbit interaction splits the highest valence bands at the K (K′) points.[3–6] When exfoliated into thin atomic layers, this band splitting opens the possibility of tuning the position of the Fermi level (*e.g.*, with a back gate voltage) toward the top spin–orbit split valence band having spin-polarized carriers. This could lead to spin-polarized carrier transport at the interface between a dielectric layer and the TMX_2, opening a new research frontier in spintronics.[7] Spin–orbit also leads to coupled valley and spin degrees of freedom due to the lack of inversion symmetry in monolayer TMX_2, and this allows optical pumping of a single valley (and spin) with circularly polarized light.[8,9] In fact, each valley has a definite chirality arising from its strong pseudo-spin–orbit coupling,[10] with the chiralities of each valley opposite each other, due to the preservation of time-reversal symmetry. This leads to possible practical ways to differentiate the two valleys and to address them individually.[10–12] It has just been demonstrated that one can optically generate valley coherent excitons in monolayer semiconductor WSe_2.[13] Most importantly, the decoherence times of the exciton valley pseudospin were found to be comparable to, or even slower than, the electron–hole recombination time, suggesting a certain robustness of the "valley index" as a result of the coupled

* Address correspondence to balicas@magnet.fsu.edu.

Received for review February 19, 2014 and accepted May 30, 2014.

Published online May 30, 2014
10.1021/nn501013c

© 2014 American Chemical Society

valley and spin degrees of freedom.[11] This suggests that similar to spins, the valley degrees of freedom could be effectively explored for novel optoelectronic devices. Since all these technologically promising effects rely on the size of the semiconducting gap and on the strong spin−orbit effect characteristic of the TMX_2 compounds, it justifies a systematic evaluation of their overall properties as a function of the atomic numbers of the composing atoms, which tunes both the size of the semiconducting gap and the strength of the spin−orbit effect. Here, we chose to evaluate the properties of α-$MoTe_2$, which is characterized by a smaller semiconducting gap in the bulk, *i.e.*, 1.0 $\pm$ 0.1 eV in contrast to 1.29 $\pm$ 0.1 eV for MoS_2,[14] and contains the 5p element Te, which is considerably heavier (by a factor of ~3.5) with respect to the 3p element S, leading to a larger splitting of the valence band, *i.e.*, 238 $\pm$ 10 meV in contrast to 161 $\pm$ 10 meV for MoS_2.[14]

To date, field-effect transistors (FETs) based on transition metal dichalcogenides (TMDs), MoS_2 in particular, were shown to display large transconductance as a function of gate voltage, significant ratios between the "on" and "off" currents (or $I_{ON}/I_{OFF} > 10^8$) owing to their large band gap (~1.2 to 1.8 eV), and a sharp conductance threshold, or "subthreshold swings" as sharp as ~60 mV/decade, thus implying an enhanced gate control. Along with these electrical properties, the planarity of the monolayers based on transition metal dichalcogenides makes their transistors viable candidates for low-power applications.[13] Furthermore, transparency, flexibility, and relative inexpensiveness make them ideal for low-cost electronics.

Besides the exploration of their remarkable optical properties, much of the current effort in the field of TMDs is devoted to the understanding of their fundamental electronic properties when exfoliated in a single or few layers. For example, when mechanically exfoliated onto SiO_2, MoS_2 and $MoSe_2$ were found to be electron-doped compounds,[15,16] in contrast to WS_2 and WSe_2, which were found to display ambipolar behavior.[17−19] This would make these latter compounds ideal for complementary digital logic applications. The combination of single-layer TMDs with dielectrics having a large dielectric constant κ such as HfO_2 or Al_2O_3 led to several reports[13,20−22] claiming a remarkable increase in carrier mobility, thus making this architecture potentially useful for liquid crystals and organic light-emitting displays.[13]

Here, we explore the electrical properties of a still less studied compound, *i.e.*, $MoTe_2$, which is characterized by a smaller semiconducting gap (0.8 or 1.24 eV when in single-layered form) relative to its S (a 3p element) or Se (a 4p element) analogues. Similarly to MoS_2 or $MoSe_2$, single atomic layers of $MoTe_2$ can be produced by using the mechanical exfoliation technique. Here, we focus on few-layered crystals mechanically exfoliated onto a 270 nm thick SiO_2 layer. Previous reports[23] found that the field-effect mobility of transition metal dichalcogenides TMDs tends to increase, reaching a maximum value when crystals are composed of approximately 10 atomic layers. A systematic study on the dependence of its properties as a function of the number of layers will be reported elsewhere, including crystals grown by transport agents other than iodine. We show that the overall performance of a $MoTe_2$-based field-effect transistor is comparable to similar devices based on MoS_2 or $MoSe_2$. However, an optical gap quite close in value to that of Si and an enhanced spin−orbit interaction (since Te is a 5p element) suggests that this compound might be particularly suitable for optoelectronic applications in a complementary range of wavelengths.

RESULTS AND DISCUSSION

Figure 1 shows a micrograph of one of our bilayered $MoTe_2$ field-effect transistors built by mechanically exfoliating $MoTe_2$ onto thermally grown 270 nm SiO_2 on Si. $MoTe_2$ crystals were grown by chemical vapor transport using iodine as the transport agent (see Methods for details). This particular $MoTe_2$ crystal is composed of a bilayered section spanning from current contact I^+ (bottom of the micrograph) up to current contact I^- and a trilayered section spanning from contact I^- up to top contact I^+. As shown below, we observed slightly higher field-effect mobility for the trilayered section when compared to the bilayered one. Here, we focus on results collected on the bilayered and trilayered material as well as on a seven-layer crystal *at room temperature* with the goal of comparing field-effect and Hall mobilities and also in order to evaluate the differences of $MoTe_2$ relative to other transition metal dichalcogenide atomic layers such as MoS_2 and $MoSe_2$.

As depicted in Figure 1a, the Hall voltage V_H, for this particular sample, was measured through voltage contacts 1 and 3 under an applied external magnetic field H, while the sample resistivity $\rho_{xx} = R_{xx}(w/l)$ (w is the channel width and l the separation of contacts) was measured through voltage leads 1 and 2 by using a conventional lock-in technique. The field-effect mobility $\mu_{FE} = (1/c_g)(d\sigma/dV_{bg})$ (c_g is the gate capacitance) is extracted by measuring the source−drain current I_{ds} as a function of the back-gate voltage V_{bg} under a constant source−drain excitation voltage V_{ds} (therefore, $\sigma = (I_{ds}/V_{ds})(L/w)$ is the two-terminal conductivity).

Figure 1b shows an atomic force microscopy (AFM) image of the $MoTe_2$ single crystal composing the FET shown in Figure 1a. The blue line depicts the line along which the height profile shown in Figure 1c was acquired, which shows a step of ~1.6 nm, a value that is quite close to that reported for the $MoTe_2$ interlayer spacing of c = 1.396 nm[24] and confirming thus that it is a bilayered crystal. The inset in Figure 1b shows an atom-resolved transmission electron microscopy image of a vapor transport grown $MoTe_2$ single crystal

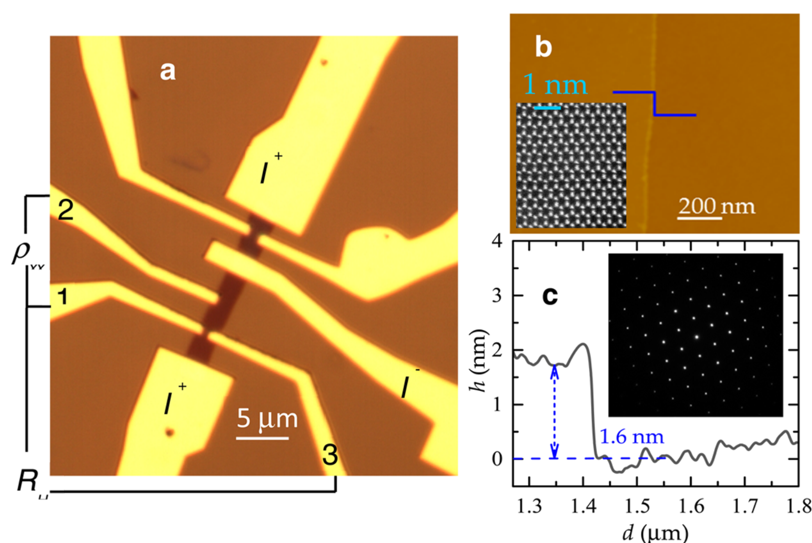

Figure 1. (a) Micrograph of one of our bilayered $MoTe_2$-based field-effect transistors mechanically exfoliated onto SiO_2. The overall length L of the channel between current contacts (labeled as I^+ and $I-$, respectively) is $L = 10.847$ μm, while its width is $w = 4.172$ μm. The resistivity ρ_{xx} is measured between voltage contacts 1 and 2 (separation $l = 1.55$ μm), while the Hall response R_H was measured through the voltage contacts 1 and 3, with magnetic field applied perpendicularly to the plane of the figure. (b) The height of the flake h is measured through an atomic force microscopy (AFM) scan long the edge of the sample (*i.e.*, along the blue line). Inset: Transmission electron microscopy image showing the atomic positions within a plane perpendicular to the interlayer direction. (c) AFM height profile along the blue line in b, indicating a flake height of ∼16 Å, which is quite close to its reported[22] interlayer distance $c = 13.964 \pm 0.004$ Å, thus indicating that this is a bilayered flake. Inset: Electron diffraction pattern showing well-defined Bragg peaks, thus confirming the high level of crystallinity for the $MoTe_2$ single crystal.

from the same synthesis batch used to fabricate the FET. For this image the electron beam flows perpendicularly to the atomic layers. In areas on the order of 100 nm^2, we could not observe any evidence for Te vacancies or domain boundaries, thus indicating a high level of uniformity and crystallinity. This is also confirmed by the diffraction pattern shown in the inset of Figure 1c, which reveals sharp Bragg peaks with no evidence for diffuse scattering.

Raman spectroscopy is a conventional and powerful tool able to identify the thickness of few-layered TMDs single crystals.[25−27] In MoS_2 the E_{2g} and A_{1g} Raman modes were shown to be particularly sensitive with respect to the number of layers, with their characteristic frequency shifting in opposite direction as the number of layers decreases.[25] Similar behavior was also identified in other TMDs such as $MoSe_2$ and WSe_2.[26,27] Here, we performed a not yet exhaustive study on the evolution of the Raman modes of $MoTe_2$ as a function of the number of layers. Figure 2a shows an AFM image of a $MoTe_2$ single crystal whose thickness varies from multiple atomic layers (outside of the scanned area) and becomes a bilayer at its right bottom edge. This crystal was used by us to collect Raman spectra as a function of the number of layers. The blue line depicts the path along which the height profile shown in Figure 2b was acquired. The height profile starts at a height of ∼1.7 nm, or approximately two atomic layers, and then increases by ∼1 nm, implying an additional atomic layer, or a triple-layered region, as the AFM tip scans from left to right along the blue line in Figure 2a. Figure 2c depicts the Raman spectra for the bulk material (magenta line, multiplied by a factor of 5) and for the areas consisting of three (blue) and two layers (red), respectively. At first glance, and in contrast with previous reports on Raman spectra on other TMDs,[25−27] the main peaks would seem to not shift in frequency as the number of layers decreases. However, by collecting Raman spectra at several points in each sample, and by averaging their position after a Lorentzian fit, one sees that the A_{1g} peak red-shifts while the E^1_g one (*i.e.*, E^1_{2g} mode in bulk crystals) blue-shifts as the number of layers decreases, similarly to what is observed in other TMDs.[25−27] After the submission of this manuscript, we became aware of a complete Raman study on α-$MoTe_2$ as a function of the number of layers by Yamamoto *et al.*[28] Our results are qualitatively similar to those reported in that manuscript, however, and on the basis of our *ab initio* density functional theory (DFT) and density functional perturbation theory (DFPT) calculations described in ref 25 for MoS_2, $MoSe_2$, and WSe_2, we index the peak at ∼290.9 cm^{-1} as the A^2_{1g} mode and not as the B^1_{2g} as implied by ref 28. The unindexed peak centered at 343.95 cm^{-1} is observed to blue-shift as the number of layers decreases. The unassigned peak seems to be a second-order resonant peak, and careful resonant Raman studies are needed to understand its nature.

Figure 3a shows the extracted drain to source current I_{ds} normalized by the width w of the channel as a function of the back-gate voltage V_{bg} and for several values of the excitation voltage V_{ds}. As seen, for gate voltages surpassing ∼20 to 30 V (depending on

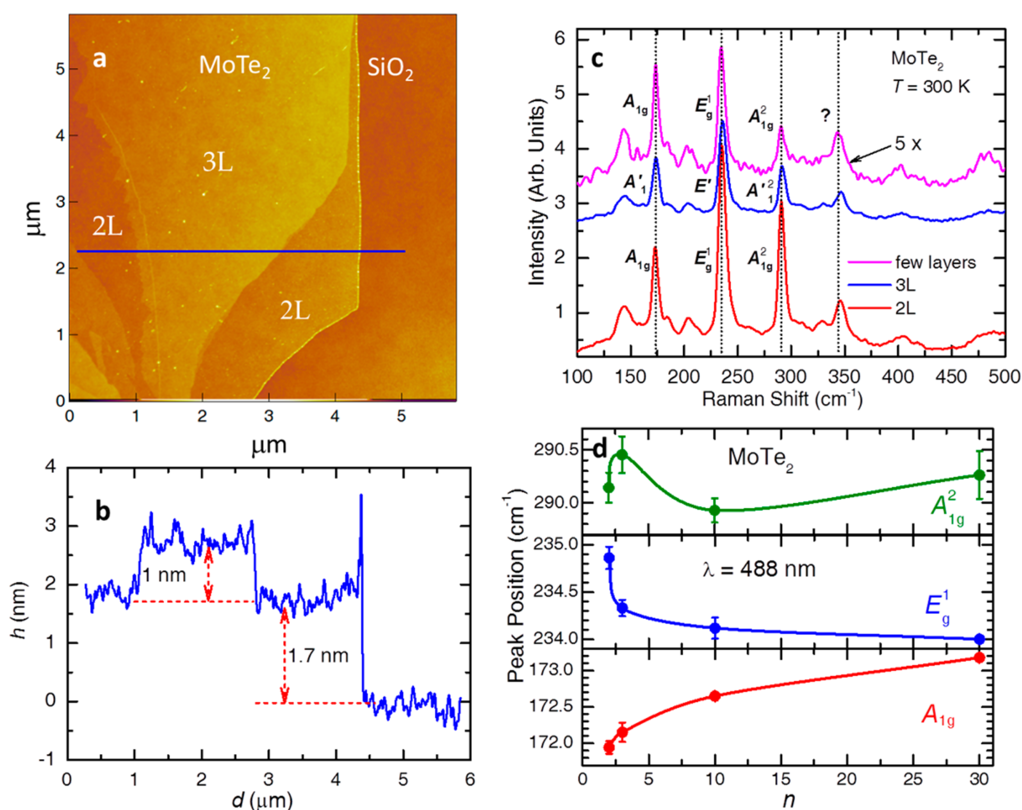

Figure 2. (a) Optical image of a $MoTe_2$ single crystalline flake, after mechanical exfoliation, used for Raman spectroscopy in conjunction with atomic force microscopy. As seen, the thickness of the flake varies, and as illustrated in b and c, certain areas of the flake are either bi- or trilayered. The blue line in b indicates the line along which we acquired the height profile displayed in c, showing areas composed of three or two atomic layers. (d) Preliminary Raman spectrum as a function of the number n of layers. The A_{1g} and the $E^1{}_g$ modes were indexed based on previous Raman studies.[26] This preliminary study indicates that the position of the A_{1g} mode (in cm^{-1}) red-shifts, while the $E^1{}_g$ is seen to "blue-shift" as the number of layers decreases. The extra sharp peaks observed in bilayers at 290.94 and ~346 cm^{-1}, respectively, are relatively close to the values of 285.9 and ~353 cm^{-1} previously reported for bilayer $MoSe_2$ and indexed as the $E^1{}_{2g}$ and a $B^1{}_{2g}$ mode, respectively. On the basis of our calculations[26] we index the 290.94 cm^{-1} peak as the $A^2{}_{1g}$ mode and leave the 353 cm^{-1} one as a peak to be indexed by future work. Notice how this last one shifts considerably as the number of layers decreases. We confirmed that similar dependence on n is also observed when using lasers with excitation wavelengths of 514 and 647 nm, respectively.

the value of V_{ds}), I_{ds} remains at the level of the noise floor of our experimental setup; hence $MoTe_2$ is a hole-doped compound. In effect, one has to reach positive gate values to "turn-off" the FET, thus indicating that this compound has an excess of holes in the conducting channel, in sharp contrast with most reports on MoS_2.[23] We verified that this behavior is intrinsic; that is, it is observed under a vacuum or helium atmosphere. Figure 3b shows the same I_{ds} as a function of V_{bg} but in a linear scale. The inset displays I_{ds} as a function of V_{bg} again but in a limited range of current and gate voltages and for an excitation voltage V_{ds} = 500 mV; from it one can extract a subthreshold swing of ~140 mV. Figure 3c plots the conductivity σ as a function of V_{bg} for each value of V_{ds} in Figure 3a and b. As seen, all curves for the different V_{ds} values collapse on a single curve, indicating that this FET behaves linearly through the entire range of V_{ds} excitations (see also the Supporting Information for leakage current as a function of back-gate voltage). The right panel of Figure 3c depicts the field-effect mobility μ_{FE} obtained, as previously mentioned, by taking the derivative of σ with respect to V_{bg} and by normalizing it with the value of the geometrical gate capacitance of SiO_2, *i.e.*, $c_g = \varepsilon_0\varepsilon_r/d = 12.783 \times 10^{-9}$ F/cm^2 (where $\varepsilon_r = 3.9$ and d = 270 nm is the SiO_2 thickness). μ_{FE} is seen to saturate at a value of ~20 cm^2/(V s), which is considerably higher than the initial reports for MoS_2 on SiO_2[29] and even 2 orders of magnitude larger than the μ_{FE} values reported for bilayered MoS_2 on SiO_2.[29,30] Although it also surpasses the overall performance of multilayered $Sn(S,Se)_2$,[31,32] these values still remain considerably lower, by two orders of magnitude, than those reported for multilayered TMDs on SiO_2[32,33] or for their single layers in conjunction with high-κ dielectrics.[21,22] Figure 3d shows I_{ds} as a function of V_{ds} for several values of the gate capacitance. As seen, the response is essentially linear, particularly at low values of V_{ds}, which is difficult to reconcile with a sizable Schottky barrier (ϕ_{SB}) at the level of the current contacts. In the text below, we show an attempt to evaluate the size of ϕ_{SB}.

Figure 4 shows results for two FETs fabricated on few-layered α-$MoTe_2$ single crystals of distinct thicknesses, *i.e.*, respectively a trilayer and a seven-layer one

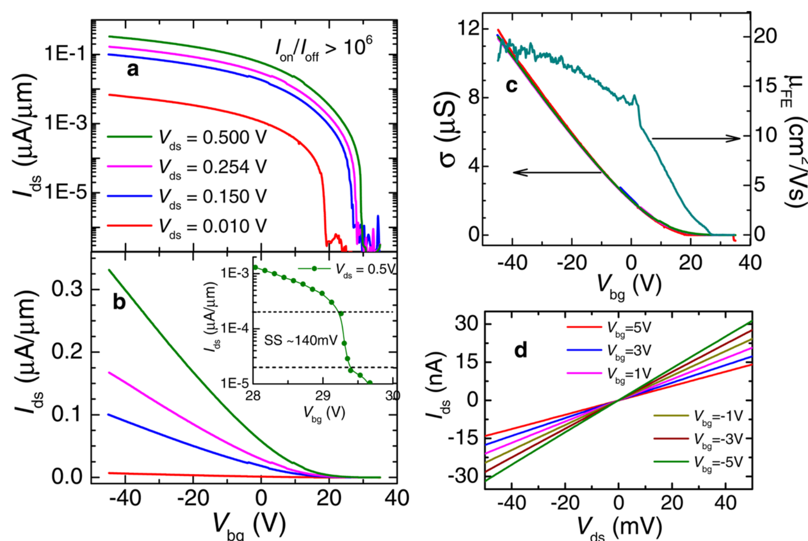

Figure 3. (a) Drain to source current I_{ds} (in a logarithmic scale) as a function of the gate voltage V_{bg} for a field-effect transistor based on bilayered $MoTe_2$ and for several values of the drain−source excitation voltage V_{ds}. A sizable current is observed for $V_{bg} < 0$ V, thus indicating that our synthetic $MoTe_2$ single crystals are hole-doped. Notice also that the ratio of "on" to "off" field-effect current is $>10^6$. (b) Same as in panel a but in a linear scale. Inset: I_{ds} as a function of V_{bg} in a limited scale, indicating a subthreshold swing SS ≈ 140 mV. (c) Right axis: Conductivity $\sigma = SL/w$, where the conductance $S = I_{ds}/V_{ds}$ as a function of V_{bg}. Left axis: Field-effect mobility $\mu_{FE} = (1/c)|d\sigma/dV_{bg}|$, where $c = \varepsilon_0\varepsilon_r/d$ is the gate capacitance (d is thickness of the SiO_2 layer) as a function of V_{bg}. (d) I_{ds} as a function of the excitation voltage V_{ds} and for several values of V_{bg}. As seen, at low excitation voltages the $I-V$ characteristic is linear.

as determined through atomic force microscopy. In effect Figure 4a shows I_{ds} as a function of V_{bg} for an FET based on a trilayered α-$MoTe_2$ crystal and for several values of the excitation voltage V_{ds}. As seen, the subthreshold swing still is sharp, but the threshold gate voltage required for current extraction increases up to ∼+40 V, suggesting a stronger level of hole dopants when compared to the bilayered crystal. Notice that this FET also shows a current on to off ratio surpassing 10^6. Figure 4b shows I_{ds} as a function of V_{bg} in a linear scale, where the red line is a linear fit from which is extracted the field-effect mobility $\mu_{FE} \approx$ 20 cm^2/(V s), which is nearly twice the value previously obtained for the bilayered FET. In order to further explore the dependence of μ_{FE} on n or the number of layers, we show in Figure 4c I_{ds} as a function of V_{bg} for a FET composed of seven layers. The same figure shows traces for increasing (red line) and decreasing (blue line) gate voltage sweeps, which do *not* reveal a sizable hysteresis. Figure 4d displays I_{ds} as a function of V_{bg} in a linear scale, from which we extract $\mu_{FE} \approx$ 27 cm^2/(V s). Therefore, similarly to what was previously reported[34] for MoS_2, the mobility of α-$MoTe_2$ increases as the number of atomic layers increases up to $n \approx 10$. Nevertheless, this mobility value is lower than the ones extracted by us[34] and other groups[35] for multilayered mechanically exfoliated MoS_2 but approaches the most recent values reported for chemical vapor deposited MoS_2.[36,37] Our energy dispersive spectroscopy (EDS) analysis (see Supporting Information) reveals ∼3% in Te excess and a similar amount of incorporated iodine. Although 3% is close to the typical EDS quantitative error bars, the lower mobilities observed here, coupled to the high levels of hole-doping, do suggest that the material is not perfectly stoichiometric. A similar situation was recently reported for natural MoS_2, where its intrinsic electron-doping was attributed to the presence of S vacancies (∼10^{13} cm^{-2}) as observed through a detailed transmission electron microscopy study.[38] At the moment, we are still examining the effect of distinct chemical transport agents with the hope of synthesizing a more stoichiometric material, since Te and iodine have contiguous atomic numbers and very similar ionic radii, which could lead to site disorder. Therefore, our results combined with those of ref 38 suggest that in TMDs a small chalcogenide deficiency or excess leads to electron- or hole-doping, respectively.

We have characterized the temperature (T) dependence of the two-terminal conductivity σ for the seven-layer α-$MoTe_2$ FET with the goal of understanding both the nature of the conduction mechanism and the quality of the contacts, or the size of the Schottky barrier at the contacts. Figure 5a shows σ in a logarithmic scale and as a function of $T^{-1/3}$. As indicated by the red lines (linear fits), for $V_{bg} \leq -10$ V the expected expression for two-dimensional variable hopping conductivity (VRH), i.e., $\sigma \propto e^{-(T_1/T)^{1/3}}$, provides an excellent description for our $\sigma(T)$, indicating a relevant role for disorder within the conducting channel. Notice that VRH-like conductivity was already previously reported for MoS_2 on SiO_2.[38,39] For $V_{bg} > -10$ V σ is better described by $\sigma \propto e^{-(T_0/T)}$, as shown in Figure 5b, implying thermally activated nearest-neighbor hopping with T_0 ranging

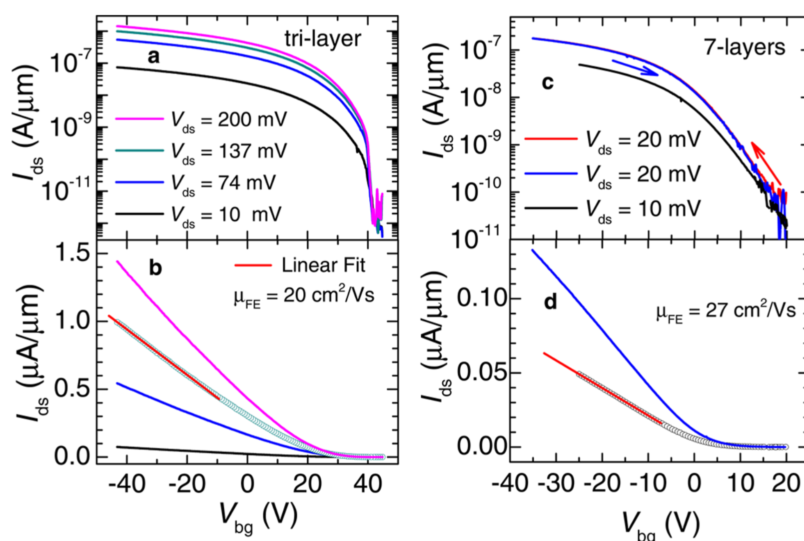

Figure 4. (a) Drain to source current I_{ds} (in a logarithmic scale) as a function of the gate voltage V_{bg} for a field-effect transistor based on a *trilayered* $MoTe_2$ crystal and for several values of the drain–source excitation voltage V_{ds}. For this particular sample, a sizable current is observed for V_{bg} < 40 V. Notice also that the on to off ratio still is >10^6, while the resulting field effect mobility $\mu_{FE} \approx 20$ cm^2/(V s) is higher than the one observed for the bilayered crystal. (b) Same as in part a but in a linear scale. (c) I_{ds} as a function of V_{bg} for a field-effect transistor based on a *seven-layer* $MoTe_2$ single crystal and for two values of the drain–source excitation voltage V_{ds}. (d) Same as in part c but in a linear scale. Red line is a linear fit from which we extract $\mu_{FE} \approx 27$ cm^2/(V s).

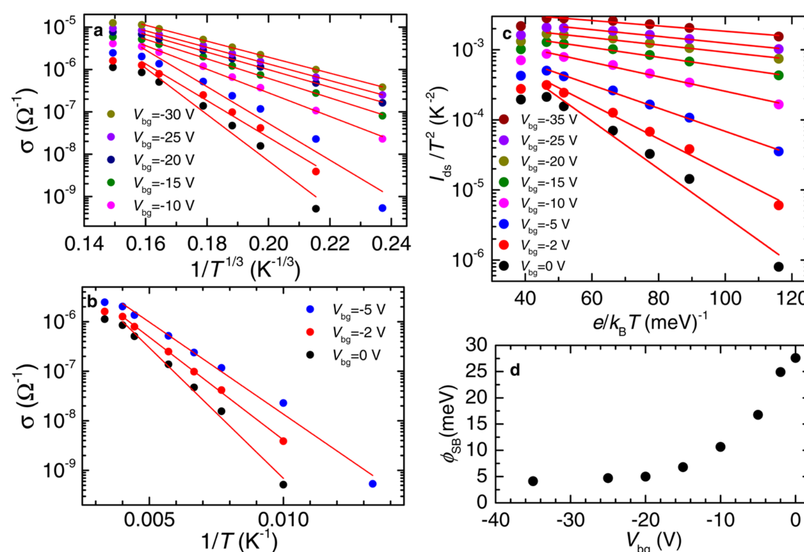

Figure 5. (a) Two-terminal conductivity $\sigma = (I_{ds}/V_{ds})(L/w)$, where L and w are the length and the width of the conducting channel, respectively, in a logarithmic scale and as a function of $T^{-1/3}$ for our *seven-layer* sample and for several values of the back-gate voltage. Red lines are linear fits indicating that two-dimensional variable range hopping conductivity describes the behavior of σ for $V_{bg} \leq -10$ V. (b) σ in logarithmic scale as a function of T^{-1}, indicating that at low gate voltages, *i.e.*, -5 V $\leq V_{bg} \leq 0$ V, σ is better described by temperature activated behavior. (c) I_{ds} normalized by the square of the temperature as a function e/k_BT. Red lines are linear fits, which according to the thermionic emission formalism would yield the size of the Schottky barrier ϕ_{SB} for carrier conduction across the current contacts. (d) ϕ_{SB} as a function of V_{bg}. Notice the quite small size of ϕ_{SB}.

from 300 to 500 K. In effect, the slope of the linear fits (red lines in Figure 5b), which yields the value of T_0, decreases with increasing V_{bg}. This is consistent with an increase in the density of states near the Fermi level[40] ε_F (since $T_0 = (k_B\varepsilon_F a)^{-1}$, where a is the average distance between defects) as one moves away from the mobility edge by sweeping the gate voltage.

Once one has acquired the two-terminal conductivity σ as a function of the T, one can proceed with another relevant exercise: to evaluate the size of the Schottky barrier for carrier conduction across the current contacts. In effect, and although Figure 3 indicates that the conductivity σ, as measured through a two-terminal configuration, is linear on excitation voltage V_{ds} when $V_{bg} > V_{bg}^{t}$, it was discussed in several

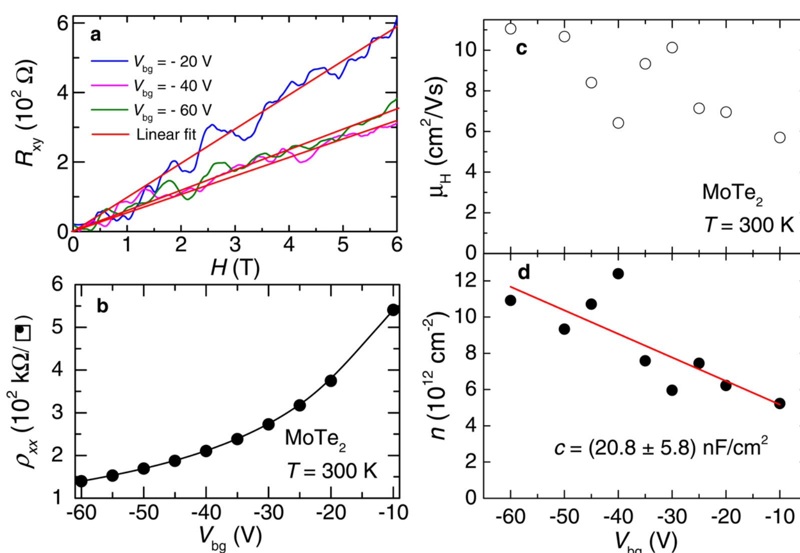

Figure 6. (a) Hall resistance R_{xy} as a function of the magnetic field H for a bilayered $MoTe_2$ FET at room temperature. Red lines are linear fits from which we extract the Hall constant $R_H = 1/ne$ (n is the density of carriers and e is the electron charges). (b) Sheet resistivity ρ_{xx} as a function of the back gate voltage V_{bg}. (c) Hall mobility $\mu_H = R_H/\rho_{xx}$ as a function of V_{bg}. (d) Carrier density $n = 1/eR_H$ as a function of V_{bg}. The red line is a linear fit from which one extracts the gate capacitance $c = ne/V_{bg}$. The extracted gate capacitance $c_g = 21 \pm 6$ nF/cm^2 is higher than the expected value for a 270 nm thick SiO_2 layer, *i.e.*, $c_g = 12.783$ nF/cm^2, indicating the presence of spurious charges in the conducting channel.

reports that the conduction through the drain and source contacts is presumably entirely dominated by Schottky barriers.[23,41] In effect, a sizable Schottky barrier $\phi_{SB} = 1.2 \pm 0.5$ eV is expected as the difference in energy between the work function of Ti, or 4.33 eV, and the electron affinity of $MoTe_2$, or 3.1 ± 0.5 eV.[42] The linear, or apparent ohmic, regime would result from thermionic emission or thermionic field emission processes. In thermionic emission theory, the drain–source current I_{ds} is related to ϕ_{SB} through the expression

$$I_{ds} = AA^*T^2 \exp(e\phi_{SB}/k_BT)$$

where A is the area of the Schottky junction, $A^* = 4\pi em^*k_B^2h^{-3}$ is the effective Richardson constant, e is the elementary charge, k_B is the Boltzmann constant, m^* is the effective mass, and h is the Planck constant.[43] In order to evaluate the Schottky barrier at the level of the contacts, in the top panel of Figure 5c we plot I_{ds} normalized by the square of the temperature T^2 as a function of e/k_BT and for several values of the gate voltage. Red lines are linear fits from which we extract the value of $\phi_{SB}(V_{bg})$. Figure 5d shows ϕ_{SB} in a logarithmic scale as a function of V_{bg}; notice the small value of $\phi_{SB} \approx 5$ meV (flat band condition), which is considerably smaller than the above estimated value exceeding 1 eV. At the moment we do not have a clear explanation for such a dramatic discrepancy; perhaps, the rather smaller values for ϕ_{SB} result from defect states relatively close to the Fermi level. Nevertheless, one has to be cautious with the extraction of the Schottky barrier through this approach, since two-terminal measurements contain contributions from both the contacts and the conduction channel, which, as discussed above, would seem to undergo disorder-induced carrier localization, thus masking the true behavior of the conduction mechanism across the contacts. Solely on the basis of the plots in Figure 5 we cannot unambiguously identify the predominant conduction mechanism. Therefore, the values of $\phi_{SB}(V_{bg})$ extracted here should be taken with caution: the very small values would imply a good band alignment between Ti and $MoTe_2$, which is difficult to conceive.

Figure 6a shows the bare Hall signal for a bilayered $MoTe_2$ FET, $R_{xy} = \Delta V_H/I = (V_H(+H) - V_H(-H))/2I$, where V_H is the voltage measured through voltage contacts 1 and 3 (see Figure 1a) as a function of the applied magnetic field H for several values of the gate voltage. From the linear fits (red lines) we extract the Hall constant $R_H = R_{xy}/H = 1/ne$, where n is the two-dimensional density of carriers. Figure 6b displays the sheet resistivity ρ_{xx} (measured through contacts 1 and 2 in Figure 1a) as a function of V_{bg}. When V_{bg} varies from -10 to -60 V, ρ_{xx} decreases from ~550 kΩ to approximately 150 kΩ. The resulting Hall mobility $\mu_H = R_H/\rho_{xx}$ is shown in Figure 5c. We note that μ_H increases from approximately 6 cm^2/(V s) to values approaching 11 cm^2/(V s). In addition, Figure 6d shows the extracted two-dimensional carrier density $n = 1/eR_H$ as a function of V_{bg}; it varies from $\sim 5 \times 10^{12}$ to $\sim 1 \times 10^{13}$ cm^{-2}. The red line represents a linear fit from which we extract the effective gate capacitance $c_g = ne/V_{bg} = 21 \pm 6$ nF/cm^2, thus indicating that the actual gate capacitance could be twice as large as the geometrical value resulting from the thickness of the SiO_2 layer (or $c_g = 12.783$ nF/cm^2). A larger experimental value for c_g can be understood as produced by spurious charges in the

conduction channel. It is noteworthy that an effectively larger experimental value for the gate capacitance would easily explain the difference between the maximum values for the field-effect and the Hall mobilities; by using the gate capacitance measured from the Hall effect in the transconductance expression used to extract the field-effect mobility, one would obtain basically the same value for both mobilities. This suggests that the electrical contacts and their respective Schottky barriers (which are rather small, as indicated in Figure 5d) do not play a determinant role in limiting the carrier mobility in our α-$MoTe_2$-based field-effect transistors.

CONCLUSIONS

$MoTe_2$ grown by chemical vapor transport using iodine as the transport agent, when mechanically exfoliated onto SiO_2 and electrically contacted by using a combination of Ti and Au, behaves as a hole-doped semiconductor in contrast to MoS_2 and $MoSe_2$. Electron dispersive spectroscopy analysis indicates the possibility of a small amount of excess Te and possibly iodine incorporation, which perhaps are the sources of hole-doping in this compound. If hole-doping resulted from Fermi level pinning associated with the metals used for the electrical contacts, it would suggest that $Mo(Se_{1-x}Te_x)_2$ or $Mo(S_{1-x}Te_x)_2$ alloys might become ambipolar, or alternatively that stacking $MoTe_2$ atomic layers onto $MoSe_2$/MoS_2 ones might also lead to ambipolar field-effect transistors, suitable for pn junctions.[45−47] Perhaps this architecture might lead to new band gap materials[44] with novel optoelectronic properties. For example, at a given layer−layer distance the holes in one atomic layer could bond to the electrons on the other one in order to create bound excitons.[45] For all three Mo compounds a systematic study on the role of specific contact metals in pinning the Fermi level either closer to the valence or to the conduction band has yet to be performed to clarify the above issues. It is also noteworthy that our $MoTe_2$ FETs display I_{ON}/I_{OFF} ratios also surpassing 10^6 and subthreshold swings of ~140 mV, which is comparable to or superior than MoS_2 or $MoSe_2$ on SiO_2 in the absence of a high-κ dielectric layer. Field-effect mobilities indicate for few layered $MoTe_2$ exfoliated onto SiO_2 carrier mobilities ranging from ~20 $cm^2/(V\ s)$ in bilayers to values approaching 30 $cm^2/(V\ s)$ in seven layers. The Hall effect, on the other hand, indicates the presence of spurious charges in the conduction channel, which certainly act as scattering centers, thus limiting the carrier mobility. Raman spectroscopy as a function of the number of layers indicates that the A_{1g} and $E^1{}_g$ modes blue-shift and red-shift, respectively, as the number of layers decreases, similarly to what was observed for other transition metal dichalcogenides. Therefore, Raman scattering can also be used in this compound in order to identify the number of layers of any given crystal.

In MoS_2 optically excited holes forming trions when bound to the photogenerated excitons were found to remain spin polarized in a given valley (for a time much longer than the trion lifetime), even in the presence of strong exchange-mediated spin relaxation processes.[11] This is claimed to result from a particular robustness of the hole valley index as the result of the coupled valley and spin degrees of freedom. In $MoTe_2$ it remains to be verified if the stronger spin−orbit/valley coupling, which was previously shown by photoemission experiments to lead to a larger valence band spin-splitting when compared to MoS_2,[14] would also lead to longer trion spin coherence times, thus making this compound particularly appealing for new photonic and optoelectronic devices.[11]

METHODS

$MoTe_2$ single crystals were synthesized through chemical vapor transport using iodine as the transport agent. The 99.999% pure Mo powder and 99.999% pure Te pellets were introduced into a quartz tube together with 99.999% pure I (5.8 mg of I per cm^3). The quartz tube was vacuumed, brought to 1150 °C, and held at this temperature for 1.5 weeks at a temperature gradient of ~100 °C. Subsequently, it was cooled to 1050 °C at a rate of 10 °C/h, followed by another cool down to 800 °C at a rate of 2 °C/h. It was held at 800 °C for 2 days and subsequently quenched in air. Bilayered flakes of $MoTe_2$ were exfoliated from these single crystals by using the "Scotch-tape" micromechanical cleavage technique and transferred onto p-doped Si wafers covered with a 270 nm thick layer of SiO_2. For making the electrical contacts 90 nm of Au was deposited onto a 4 nm layer of Ti *via* e-beam evaporation. Contacts were patterned using standard e-beam lithography techniques. After gold deposition, the devices were annealed at 250 °C for ~2 h in forming gas. This was subsequently followed by high-vacuum annealing for 24 h at 120 °C. Atomic force microscopy imaging was performed using the Asylum Research MFP-3D AFM. Electrical characterization was performed by using a combination of sourcemeter (Keithley 2612 A), lock-in amplifier (Signal Recovery 7265), and resistance bridges (Lakeshore 370) coupled to a physical property measurement system. The Raman spectra were measured in a backscattering geometry using a 488 nm laser excitation wavelength. Sub-angström aberration-corrected transmission electron microscopy was performed by using a JEM-ARM200cF microscope. EDS was performed through field-emission scanning electron microscopy (Zeiss 1540 XB).

Conflict of Interest: The authors declare no competing financial interest.

Acknowledgment. This work was supported by the U.S. Army Research Office MURI Grant No. W911NF-11-1-0362. The NHMFL is supported by NSF through NSF-DMR-0084173 and the State of Florida.

Supporting Information Available: Leakage current $I_{Leakage}$ flowing through the $MoTe_2$/SiO_2 interface as a function of back gate voltage V_{bg}, indicating that the drain to source current extracted from a typical $MoTe_2$ FET is intrinsic to the interface. Typical EDS spectra of a chemical vapor transport grown $MoTe_2$ single crystal. This material is available free of charge *via* the Internet at http://pubs.acs.org.

REFERENCES AND NOTES

1. Chhowalla, M.; Shin, H. S.; Eda, G.; Li, L.-J.; Loh, K. P.; Zhang, H. The Chemistry of Two-Dimensional Layered Transition Metal Dichalcogenide Nanosheets. *Nat. Chem.* **2013**, *5*, 263–275.
2. Mak, K. F.; Lee, C.; Hone, J.; Shan, J.; Heinz, T. F. Atomically Thin MoS_2: A New Direct-Gap Semiconductor. *Phys. Rev. Lett.* **2010**, *105*, 136805.
3. Bishop, N. C.; Padmanabhan, M.; Vakili, K.; Shkolnikov, Y. P.; De Poortere, E. P.; Shayegan, M. Valley Polarization and Susceptibility of Composite Fermions around a Filling Factor $\nu = 3/2$. *Phys. Rev. Lett.* **2007**, *98*, 266404.
4. Zhu, Z.; Collaudin, A.; Fauque, B.; Kang, W.; Behnia, K. Field-Induced Polarization of Dirac Valleys in Bismuth. *Nat. Phys.* **2012**, *8*, 89–94.
5. Rycerz, A.; Tworzydlo, J.; Beenakker, C. W. J. Valley Filter and Valley Valve in Graphene. *Nat. Phys.* **2007**, *3*, 172–175.
6. Gupta, J. A.; Knobel, R.; Samarth, N.; Awschalom, D. D. Ultrafast Manipulation of Electron Spin Coherence. *Science* **2001**, *292*, 2458–2461.
7. Li, X.; Zhang, F.; Niu, Q. Unconventional Quantum Hall Effect and Tunable Spin Hall Effect in Dirac Materials: Application to an Isolated MoS_2 Trilayer. *Phys. Rev. Lett.* **2013**, *110*, 066803.
8. Xiao, D.; Yao, W.; Niu, Q. Valley-Contrasting Physics in Graphene: Magnetic Moment and Topological Transport. *Phys. Rev. Lett.* **2007**, *99*, 236809.
9. Sugai, S.; Ueda, T.; Murase, K. Raman Scattering in MoS_2, $MoSe_2$ and α-$MoTe_2$. *J. Phys. Colloques* **1981**, *42*, 320–322.
10. Xiao, D.; Liu, G.-B.; Feng, W.; Xu, X.; Yao, W. Coupled Spin and Valley Physics in Monolayers of MoS_2 and Other Group-VI Dichalcogenides. *Phys. Rev. Lett.* **2012**, *108*, 196802.
11. Mak, K.F.; He, K.; Lee, C.; Lee, G. H.; Hone, J.; Heinz, T. F.; Shan, J. Tightly Bound Trions in Monolayer MoS_2. *Nat. Mater.* **2013**, *12*, 207–211.
12. Jones, A. M.; Yu, H.; Ghimire, N. J.; Wu, S.; Aivazian, G.; Ross, J. S.; Zhao, B.; Yan, J.; Mandrus, D. G.; Xiao, D.; Yao, W.; Xu, X. Optical Generation of Excitonic Valley Coherence in Monolayer WSe_2. *Nat. Nanotechnol.* **2013**, *8*, 634–638.
13. Kim, S.; Konar, A.; Hwang, W. S.; Lee, J. H.; Lee, J.; Yang, J.; Jung, C.; Kim, H.; Yoo, J. B.; Choi, J. Y.; Kim, K.; *et al.* High-Mobility and Low-Power Thin-Film Transistors Based on Multilayer MoS_2 Crystals. *Nat. Commun.* **2012**, *3*, 101.
14. Böker, Th.; Severin, R.; Müller, A.; Janowitz, C.; Manzke, R.; Voß, D.; Krüger, P.; Mazur, A.; Pollmann, J. Band Structure of MoS_2, $MoSe_2$, and α-$MoTe_2$: Angle-Resolved Photoelectron Spectroscopy and ab Initio Calculations. *Phys. Rev. B* **2001**, *64*, 235305.
15. Radisavljevic, B.; Radenovic, A.; Brivio, J.; Giacometti, V.; Kis, A. Single-Layer MoS_2 Transistors. *Nat. Nanotechnol.* **2011**, *6*, 147.
16. Larentis, S.; Fallahazad, B.; Tutuc, E. Field-Effect Transistors and Intrinsic Mobility in Ultra-Thin $MoSe_2$ Layers. *Appl. Phys. Lett.* **2012**, *101*, 223104.
17. Podzorov, V.; Gershenson, M. E.; Kloc, Ch.; Zeis, R.; Bucher, E. High-Mobility Field-Effect Transistors Based on Transition Metal Dichalcogenides. *Appl. Phys. Lett.* **2004**, *84*, 3301.
18. Hwang, W. S.; Remskar, M.; Yan, R.; Protasenko, V.; Tahy, K.; Chae, S. D.; Zhao, P.; Konar, A.; Xing, H.; Seabaugh, A.; Jena, D. Transistors with Chemically Synthesized Layered Semiconductor WS_2 Exhibiting 10^5 Room Temperature Modulation and Ambipolar Behavior. *Appl. Phys. Lett.* **2012**, *101*, 013107.
19. Das, S.; Appenzeller, J. WSe_2 Field-Effect Transistors with Enhanced Ambipolar Characteristics. *Appl. Phys. Lett.* **2013**, *103*, 103501.
20. Fang, H.; Chuang, S.; Chang, T. C.; Takei, K.; Takahashi, T.; Javey, A. High-Performance Single Layered WSe_2 p-FETs with Chemically Doped Contacts. *Nano Lett.* **2012**, *12*, 3788–3792.
21. Radisavljevic, B.; Kis, A. Mobility Engineering and a Metal-Insulator Transition in Monolayer MoS_2. *Nat. Mater.* **2013**, *12*, 815–820.
22. Baugher, B. W. H.; Churchill, H. O. H.; Yang, Y.; Jarillo-Herrero, P. Intrinsic Electronic Transport Properties of High-Quality Monolayer and Bilayer MoS_2. *Nano Lett.* **2013**, *13*, 4212.
23. Das, S.; Chen, H.-Y.; Penumatcha, A. V.; Appenzeller, J. High Performance Multilayer MoS_2 Transistors with Scandium Contacts. *Nano Lett.* **2013**, *13*, 100–105.
24. Puotinen, D.; Newham, R. E. The Crystal Structure of $MoTe_2$. *Acta Crystallogr.* **196**, *14*, 691–692.
25. Lee, C.; Yan, H.; Brus, L. E.; Heinz, T. F.; Hone, J.; Ryu, S. Anomalous Lattice Vibrations of Single- and Few-Layer MoS_2. *ACS Nano* **2010**, *4*, 2695–2700.
26. Terrones, H.; Del Corro-Garcia, E.; Feng, S.; Poumirol, J. M.; Rhodes, D.; Smirnov, D.; Pradhan, N. R.; Lin, Z.; Nguyen, M. A. T.; Elías, A. L.; *et al.* New First Order Raman-Active Modes in Few Layered Transition Metal Dichalcogenides. *Sci. Rep.* **2014**, *4*, 4215.
27. Tonndorf, P.; Schmidt, R.; Bottger, P.; Zhang, X.; Borner, J.; Liebig, A.; Albrecht, M.; Kloc, C.; Gordan, O.; Zahn, D. R. T.; *et al.* Photoluminescence Emission and Raman Response of Monolayer MoS_2, $MoSe_2$, and WSe_2. *Opt. Express* **2013**, *21*, 4908–4916.
28. Yamamoto, M.; Wang, S. T.; Ni, M.; Lin, Y.-F.; Li, S.-L.; Aikawa, S.; Jian, W.-B.; Ueno, K.; Wakabayashi, K.; Tsukagoshi, K. Strong Enhancement of Raman Scattering from a Bulk-Inactive Vibrational Mode in Few-Layer $MoTe_2$. *ACS Nano* **2014**, *8*, 3895–3903.
29. Novoselov, K. S.; Jiang, D.; Schedin, F.; Booth, T. J.; Khotkevich, V. V.; Morozov, S. V.; Geim, A. K. Two-Dimensional Atomic Crystals. *Proc. Natl. Acad. Sci. U.S.A.* **2005**, *102*, 10451.
30. Qiu, H.; Pan, L. J.; Yao, Z.N.; Li, J. J.; Shi, Y.; Wang, X. R. Electrical Characterization of Back-Gated Bi-Layer MoS_2 Field-Effect Transistors and the Effect of Ambient on Their Performances. *Appl. Phys. Lett.* **2012**, *100*, 123104.
31. Su, Y.; Ebrish, M. A.; Olson, E. J.; Koester, S. J. $SnSe_2$ Field-Effect Transistors with High Drive Current. *Appl. Phys. Lett.* **2013**, *103*, 63104.
32. De, D.; Manongdo, J.; See, S.; Zhang, V.; Guloy, A.; Peng, H. High On/Off Ratio Field Effect Transistors Based on Exfoliated Crystalline SnS_2 Nano-Membranes. *Nanotechnology* **2013**, *24*, 025202.
33. Ayari, A.; Cobas, E.; Ogundadegbe, O.; Fuhrer, M. S. Realization and Electrical Characterization of Ultrathin Crystals of Layered Transition-Metal Dichalcogenides. *J. Appl. Phys.* **2007**, *101*, 014507.
34. Pradhan, N. R.; Rhodes, D.; Zhang, Q.; Talapatra, S.; Terrones, M.; Ajayan, P. M.; Balicas, L. Intrinsic Carrier Mobility of Multi-Layered MoS_2 Field-Effect Transistors on SiO_2. *Appl. Phys. Lett.* **2013**, *102*, 123105.
35. Das, S.; Chen, H.-Y.; Penumatcha, A. V.; Appenzeller, J. High Performance Multilayer MoS_2 Transistors with Scandium Contacts. *Nano Lett.* **2013**, *13*, 100–105.
36. Zhu, W.; Low, T.; Lee, Y.-H.; Wang, H.; Farmer, D. B.; Kong, J.; Xia, F.; Avouris, P. Electronic Transport and Device Prospects of Monolayer Molybdenum Disulphide Grown by Chemical Vapour Deposition. *Nat. Commun.* **2014**, *5*, 3087.
37. Liu, H.; Si, M.; Najmaei, S.; Neal, A.T.; Du, Y.; Ajayan, P. M.; Lou, J.; Ye, P. D. Statistical Study of Deep Submicron Dual-Gated Field-Effect Transistors on Monolayer Chemical Vapor Deposition Molybdenum Disulfide Films. *Nano Lett.* **2013**, *13*, 2640–2646.
38. Qiu, H.; Xu, T.; Wang, Z.; Ren, W.; Nan, H.; Ni, Z.; Chen, Q.; Yuan, S.; Miao, F.; Song, F.; *et al.* Hopping Transport through Defect-Induced Localized States in Molybdenum Disulphide. *Nat. Commun.* **2013**, *4*, 2642.
39. Ghatak, S.; Pal, A. N.; Ghosh, A. Nature of Electronic States in Atomically Thin MoS_2 Field-Effect Transistors. *ACS Nano* **2011**, *5*, 7707–7712.
40. Mott, N. F. *Electronic Processes in Non-Crystalline Materials*; Clarendon Press: Oxford, UK, 1979.
41. Chen, J.-R; Odenthal, P. M.; Swartz, A.G.; Floyd, G.C.; Wen, H.; Luo, K.Y.; Kawakami, R. K. Control of Schottky Barriers in Single Layer MoS_2 Transistors with Ferromagnetic Contacts. *Nano Lett.* **2013**, *13*, 3106–3110.
42. Loher, T.; Tomm, Y.; Pettenkofer, C.; Klein, A.; Jaegermann, W. Structural Dipoles at Interfaces Between Polar II–VI Semiconductors CdS and CdTe and Non-Polar Layered Transition Metal Dichalcogenide Semiconductors $MoTe_2$ and WSe_2. *Semicond. Sci. Technol.* **2000**, *15*, 514–522.

43. Yang, H.; Heo, J.; Park, S.; Song, H. J.; Seo, D. H.; Byun, K.-E.; Kim, P.; Yoo, I.; Chung, H.-J.; Kim, K. Graphene Barristor, a Triode Device with a Gate-Controlled Schottky Barrier. *Science* **2012**, *336*, 1140.
44. Terrones, H.; Lopez-Urias, F.; Terrones, M. Novel Hetero-Layered Materials with Tunable Direct Band Gaps by Sandwiching Different Metal Disulfides and Diselenides. *Sci. Rep.* **2013**, *3*, 1549.
45. Lee, C.-H.; Lee, G.-H.; van der Zande, A. M.; Chen; Li, Y.; Han, M.; Cui, X.; Arefe, G.; Nuckolls, C.; Heinz, T. F.; Guo, J.; Hone, J.; Kim, P. Atomically Thin P-N Junctions with Van Der Waals Heterointerfaces. 2014, arXiv: physics/1403.3062. arXiv.org e-Print archive http://arxiv.org/abs/1403.3062 (accessed Mar 21, 2014).
46. Pospischil, A.; Furchi, M. M.; Mueller, T. Solar Energy Conversion and Light Emission in An Atomic Monolayer P-N Diode. *Nat. Nanotechnol.* **2014**, *9*, 257–261.
47. Baugher, B. W. H.; Churchill, H. O. H.; Yang, Y.; Jarillo-Herrero, P. Optoelectronics with Electrically Tunable PN Diodes in a Monolayer Dichalcogenide. *Nat. Nanotechnol.* **2014**, *9*, 262–267.